# Optical power equalization using Fabry-Perot semiconductor optical amplifier

**Yun Ling (凌 云), Kun Qiu (邱 昆), Wei Zhang (张 薇), and Ying Pang (庞 莹)**

*Key Laboratory of Broadband Optical Fiber Transmission and Communication Networks, University of Electronic Science and Technology of China, Chengdu 610054*

Received July 14, 2006

A novel scheme of optical power equalization based on Fabry-Perot semiconductor optical amplifier (FP-SOA) is proposed. Because of the gain characteristic of FP-SOA, real-time controlling mechanism according to input optical power is aborted in the scheme. The simulations show that 10-dB pulse peak power variation can be clamped in less than 1 dB. The influences of injecting current, pulse periods, and pulse width are discussed.

*OCIS codes:* 060.0060, 060.2330, 060.4370.

Optical packet switching (OPS) technology will conquer the electronic bottleneck in the O/E/O switching nodes and provide the smaller switching granularity than wavelength switching[1−6]. But there still exist many problems handicapping the realization of OPS, for example, reducing the optical packet power variation. In optical packet switching networks, optical packets are routed individually according to generalized multiprotocol label switching (GMPLS) and experience the different loss in the diverse transmission paths. In the core switching nodes, the packets will suffer optical signal processing including the wavelength conversion, fiber delay lines (FDLs), optical regeneration and so on. According to the scheduling mechanism, some optical packets experience the more components and others experience less. The optical packet power will vary each other and the dramatic value of power variations between the consecutive packets can reach higher than 10 dB[7]. Since wavelength conversion, optical clock recovery and optical regeneration can work well only when the optical power of input signal falls in the certain range, the dramatic power variation will invalidate the optical signal processing function in the core switching nodes. Otherwise, the burst receiving will put stringent requirement on the dynamic range of the receiver and increase the bit error probability in the edge nodes. Optical power equalizer eliminates the power variation and clamps the power fluctuation in a small range. Several approaches have been proposed including the use of saturated semiconductor optical amplifier (SOA)[7] with opto-electronic[8,9] or all-optical[10] control. According to the controlling mechanisms, they can be divided into three types: 1) controlling the gain by adjusting the bias current; 2) using the saturation effect and controlling the optical power of continuous wave on another wavelength to adjust the gain of signal wave; 3) using the wavelength conversion and controlling the power of the pump light.

To obtain the controlling information, the input optical power has to be estimated by taping a portion of incident light before the lights come into the equalizer in these schemes. The real-time control will increase the complexity of the system and impose the processing delay. The rise time and fall time of the electronic controlling signal (about tens of microseconds[9]) will also limit the equalizing speed.

We have proposed a kind of optical power equalizer based on SOA-based Mach-Zehnder interferometer (SOA-MZI) structure without any dynamic control[11]. Here, we propose another scheme of optical power equalization using Fabry-Perot (FP-SOA). As shown in Fig. 1, only one FP-SOA is enough to clamp different powers of input optical packets to a certain value without any feedback control.

The gain of FP-SOA can be expressed as[12]

$$G = \frac{(1-R_1)(1-R_2)G_{\rm s}}{(1-\sqrt{R_1R_2}G_{\rm s})^2 + 4\sqrt{R_1R_2}G_{\rm s}\sin^2\phi}, \tag{1}$$

where $R_1$ and $R_2$ are the facet reflectivities. The single pass gain $G_{\rm s}$ and phase $\phi$ under the assumption of uniform carrier distribution can be expressed as

$$G_{\rm s} = \exp\left\{[\Gamma a(N-N_{\rm tr})-\alpha]L\right\}, \tag{2}$$

$$\phi = \frac{2\pi}{\lambda}nL, \tag{3}$$

where $\Gamma$ is the optical confinement factor, $a$ the linear material gain coefficient, $N$ the carrier density, $N_{\rm tr}$ the carrier density at transparency, $\alpha$ the loss coefficient, $L$ the cavity length, $\lambda$ the wavelength, and $n$ the equivalent refractive index. The equivalent refractive index $n$ is relative to the carrier density $N$. In general, $n$ is modeled as a linear function of carrier density

$$n = n_0 + \frac{{\rm d}n}{{\rm d}N}N, \tag{4}$$

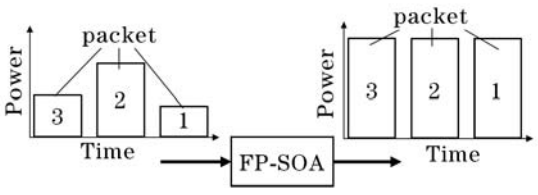


Fig. 1. FP-SOA optical power equalizer.

where $n_0$ is the equivalent refractive index at zero carrier density, $\mathrm{d}n/\mathrm{d}N$ is the differential of equivalent refractive index with respect to carrier density.

From Eq. (1) to Eq. (4), it is easy to be found that the gain of FP-SOA not only has the wavelength selectivity but also fluctuates with the carrier density. Figure 2(a) shows the relationship between the gain $G$ and carrier density $N$ when $R_1 = R_2 = 0.1$, $L = 0.5$ mm, $\Gamma = 0.1$, and $\lambda = 1.55$ $\mu$m. When $N = 2.478 \times 10^{24}$ m$^{-3}$, the gain reaches to 18.9 dB. When $N = 2.53 \times 10^{24}$ or $2.42 \times 10^{24}$ m$^{-3}$, the gain falls to $-3$ dB. For realizing optical power equalization, FP-SOA is required to work in region I as shown in Fig. 2(a). In region I, the gain decreases with the depletion of carrier density. Especially, it is the steep gain decreasing on FP-SOA that makes the gain sensitive to the optical power. Since higher input optical power will deplete more carriers and lead to lower level of carrier density, the corresponding gain is lower. On the contrary, lower input optical power will lead to higher level of carrier density and achieve relatively higher gain. For example, the input optical power, $P_A < P_B < P_C < P_D$, will deplete the carrier, cause the carrier density $N_A > N_B > N_C > N_D$, and achieve the corresponding gain $G_A > G_B > G_C > G_D$ (as shown in Fig. 2(a)). By optimizing the FP-SOA parameters and adjusting the the slope curve of $G$ versus $N$ to satisfy $P_A\,(\mathrm{dBm}) + G_A\,(\mathrm{dB}) \approx P_B\,(\mathrm{dBm}) + G_B\,(\mathrm{dB}) \approx P_C\,(\mathrm{dBm}) + G_C\,(\mathrm{dB}) \approx P_D\,(\mathrm{dBm}) + G_D\,(\mathrm{dB})$, the variable-power input optical signal will be clamped to almost the constant output power. The relation curve of input optical power $P_{\mathrm{in}}$ (dBm) and the gain $G$ (dB) for the ideal optical power equalizer where $P_{\mathrm{in}}\,(\mathrm{dBm}) + G\,(\mathrm{dB}) = \mathrm{constant}$, is a straight line with the differential ratio of $-1$. This rule can be one of the standards to evaluate the performance of optical power equalizer. It can also be used to find the equalization range of input optical power.

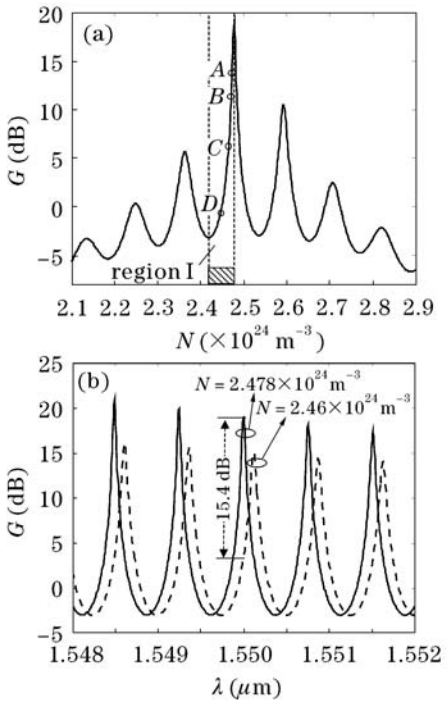


Fig. 2. Gain $G$ versus carrier density $N$ (a) and wavelength $\lambda$ (b).

The gain variation with the carrier density can also be explained from the gain spectra of FP-SOA as shown in Fig. 2(b). When $N = 2.478 \times 10^{24}$ m$^{-3}$, the gain peak appears at the wavelength of 1.55 $\mu$m. Since the refractive index in the active region increases with the carrier depletion, the gain spectrum of FP-SOA will shift toward longer wavelength. When $N = 2.46 \times 10^{24}$ m$^{-3}$, the gain at the wavelength of 1.55 $\mu$m is reduced to 3.5 dB. From the multi-peak gain spectrum of FP-SOA in Fig. 2(b), the function of optical power equalization can be realized at the periodical wavelength for a certain carrier density, i.e., a certain injecting current.

For researching the dynamic characteristic of pulse amplification in FP-SOA and verifying the feasibility of optical power equalization using FP-SOA, a numerical model is established according to Refs. [13] and [14]. In the simulation, $R_1 = R_2 = 0.1$, $L = 0.5$ mm, $\lambda = 1.55$ $\mu$m, $\Gamma = 0.1$, and other parameters are adopted as shown in Ref. [13].

Figure 3 shows the input and output pulse waveforms and the variation of carrier density when the injecting current $I = 61.8$ mA. The injecting current $I = 61.8$ mA guarantees FP-SOA working in region I. For simplicity, four-pulse train is adopted to represent a packet and the pulses have Gaussian waveforms. The peak power of the packets varies from $-17.5$ to $-7.5$ dBm, the pulse period is 0.708 ns and the full width at half maximum (FWHM) is 147.4 ps. After the packets pass through FP-SOA, the peak power is clamped between $-7.8$ and $-6.2$ dBm. The corresponding variation of carrier density also indicates that the carrier density shifts to lower values with the peak power increasing.

Figure 4(a) shows the relationship between output pulse peak power $P_{\mathrm{out}}$ and input pulse peak power $P_{\mathrm{in}}$ in different kinds of injecting currents. 10-dB variation of $P_{\mathrm{in}}$ can be clamped into less than 1 dB. With the increase of injecting current, the working point shifts to higher carrier density and the higher gain is achieved in region I. Because of the different working points in the different injecting currents, the differential ratios of corresponding relationship curves of $P_{\mathrm{out}}$ and $P_{\mathrm{in}}$ will be distinguished but not dramatic. When $I = 62.0$ mA, $P_{\mathrm{in}}$ less than $-18$ dBm induces the working point to shift to the right side of region I and locate in the falling slope of the $G$ versus $N$ curve. So the sharp increasing of $P_{\mathrm{out}}$ appears under this condition. Figure 4(b) shows the relationship

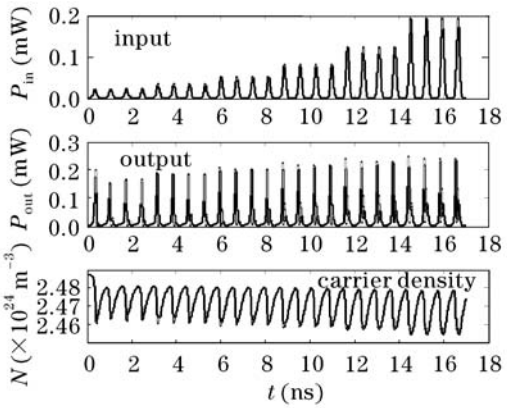


Fig. 3. Input and output waveforms and the corresponding variation of carrier density.

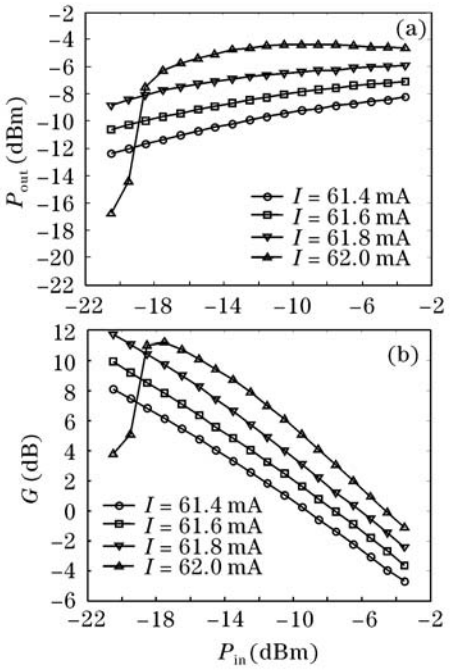


Fig. 4. Influence of injecting current.

between the peak gain $G$ and $P_{\rm in}$. There appears a gain peak corresponding to the gain peak in the $G$ versus $N$ relationship as $I = 62.0$ mA. It also explains that $P_{\rm in}$ less than $-18$ dBm shifts the working point to the right side of the $G$ versus $N$ gain peak, where $G$ increases with the carrier depletion. Figure 4(b) also shows that the optical power clamping range shifts toward higher power when the injecting current is increasing.

Because of relatively slow carrier recovery in SOA, the data rate is confined. The pulse periods will influence the carrier density that recovers from the leading pulse. Since the gain depends on the carrier density, the pulse periods

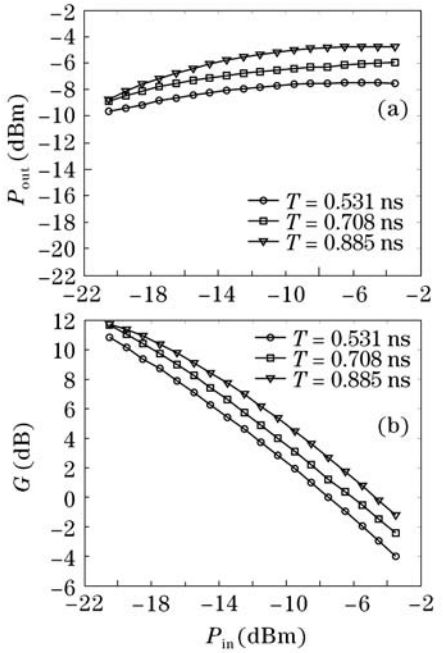


Fig. 5. Influence of pulse period ($I = 61.8$ mA, pulse width $W = 147.4$ ps).

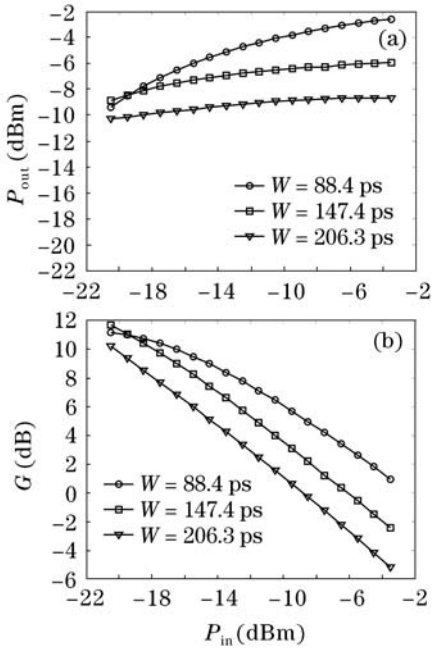


Fig. 6. Influence of pulse width ($I = 61.8$ mA, pulse period $T = 0.708$ ns).

will affect the performance of optical power equalization. Figure 5(a) shows the relationship between $P_{\rm out}$ and $P_{\rm in}$ and Fig. 5(b) shows the relationship between $G$ and $P_{\rm in}$ in various pulse periods. By decreasing the pulse period, the gain decreases due to not completely carrier recovery. But the output power variation is also reduced at the same time. The optical power clamping range shifts toward lower power when the pulse period becomes small. It needs to point out that too small pulse period will degrade the extinction ratio of the pulses after FP-SOA. So there exists an optimum pulse period.

Figure 6(a) shows the relationship between $P_{\rm out}$ and $P_{\rm in}$ and Fig. 6(b) shows the relationship between $G$ and $P_{\rm in}$ in various pulse widths. Wider pulses achieve lower gain but have flat $P_{\rm out}$ for a large range of $P_{\rm in}$, as shown in Fig. 6(a). Figure 6(b) indicates that the optical power clamping range shifts toward lower power with the increase of pulse width. It can be explained that wide pulses require less peak power than narrow pulse for depleting the same number of the carrier.

In conclusion, due to the steep gain characteristic of FP-SOA, optical power equalization can be realized by setting the working points in region I. This scheme has not any requirement of feedback control. The simulation verifies the feasibility of the scheme. Increasing injecting current or pulse period or decreasing pulse width shifts the optical power clamping range toward higher power. Relatively small pulse period and large pulse width provide flat output power.

This work was supported by the National Natural Science Foundation of China under Grant No. 60572008. Y. Ling's e-mail address is hello_lingyun@163.com.

## References

1. F. Ramos, E. Kehayas, J. M. Martinez, R. Clavero, J. Marti, L. Stampoulidis, D. Tsiokos, H. Avramopoulos, J.

Zhang, P. V. Holm-Nielsen, N. Chi, P. Jeppesen, N. Yan, I. T. Monroy, A. M. J. Koonen, M. T. Hill, Y. Liu, H. J. S. Dorren, R. V. Caenegem, D. Colle, M. Pickavet, and B. Riposati, J. Lightwave Technol. **23,** 2993 (2005).

2. Z. Pan, H. Yang, J. Yang, J. Hu, Z. Zhu, J. Cao, K. Okamoto, S. Yamano, V. Akella, and S. J. B. Yoo, J. Lightwave Technol. **23,** 3270 (2005).
3. W. A. Vanderbauwhede and D. A. Harle, J. Lightwave Technol. **23,** 2215 (2005).
4. B. A. Small, T. Kato, and K. Bergman, IEEE Photon. Technol. Lett. **17,** 2472 (2005).
5. A. M. J. Koonen, J. J. V. Olmos, I. T. Monroy, J. G. J. Jennen, C. Peucheret, E. van Breusegem, and E. Zouganeli, in *Proceedings of ECOC2005* Mo4.4.1 (2005).
6. H. Uenohara, S. Shimizu, and K. Kobayashi, in *Proceedings of ECOC2005* Th3.4.1 (2005).
7. D. Chiaroni, N. L. Sauze, T. Zami, and J. Y. Emery, in *Proceedings of ECOC2001* We.B.2.6 (2001).
8. H. Wessing, B. Sorensen, B. Lavigne, E. Balmefrezol, and O. Leclere, in *Proceedings of OFC2004* WD2 (2004).
9. A. V. Tran, C.-J. Chae, and R. S. Tucker, in *Proceedings of OFC2005* OME46 (2005).
10. J. L. Jackel, T. C. Banwell, S. R. McNown, and J. A. Perreault, in *Proceedings of ECOC2001* We.B.3.6 (2001).
11. Y. Ling, K. Qiu, P. Liu, and Y. Wang, in *Proceedings of ICOCN2005* 237 (2005).
12. P. Brosson, J. Lightwave Technol. **12,** 49 (1994).
13. M. J. Connelly, IEEE J. Quantum Electron. **37,** 439 (2001).
14. M. J. Connelly, IEE Proc. Circuits Devices Syst. **149,** 173 (2002).